Carbon Nanotube - Silicon Solar Cells

Kehang Cui[1,2] and Shigeo Maruyama[2,3*]

[1] Department of Mechanical Engineering, Massachusetts Institute of Technology, 77 Massachusetts Avenue, Cambridge, MA 02139, USA

[2] Department of Mechanical Engineering, The University of Tokyo, 7-3-1 Hongo, Bunkyo-ku, Tokyo 113-8656, Japan

[3] Energy NanoEngineering Laboratory, National Institute of Advanced Industrial Science and Technology (AIST), 1-2-1 Namiki, Tsukuba 305-8564, Japan

* Corresponding Author:

Shigeo Maruyama, maruyama@photon.t.u-tokyo.ac.jp, Department of Mechanical Engineering, The University of Tokyo, 7-3-1 Hongo, Bunkyo-ku, Tokyo 113-8656, Japan; Tel: +81-3-5841-6421; Fax: +81-3-5800-6983.

The one-dimensional electronic structure of single-walled carbon nanotubes (SWNTs) provides appealing properties including excellent optical, electrical, mechanical and thermal properties [1]. Specifically, for the light harvesting applications, SWNTs have the superiorities in terms of the wide spectrum of absorption ranging from near-infrared to visible wavelength, high electrical conductivity at high transparency as well as the possible multiple exciton generation. Combined with earth abundance and chemical stability, a film made of SWNTs is a very promising candidate for next-generation solar cell applications. However, two main challenges have been hindering the full exploitation of SWNTs for the solar cell applications: (1) the properties of SWNT assemblies are less superior to those of the individual SWNTs; (2) the technique of assembling SWNTs to photovoltaic devices needs further investigation and understanding. We will introduce these challenges in SWNT/Si solar cells and will briefly introduce the multi-functional polymer coating technique. The graphene/Si solar cells using large-scale single-crystal graphene is also discussed. Finally, applications of films of SWNTs to organic thin film solar cells (OSC) and perovskite solar cells are briefly introduced.

Silicon solar cells are so far the most mature technology among all photovoltaics with the PCE of 24.7% [2] achieved in laboratory and 13 – 17% for modules [3], which is approaching the Shockley-Queisser limit. However, the manufacturing cost of crystalline silicon solar cells is very high, of which the most expensive process is the fabrication of silicon wafer and high-temperature phosphorus diffusion doping process to form *p*-*n* junction. The emerging next-generation solar cells are attracting wide-spread interest because of the significantly reduced manufacturing cost and high efficiency. Recently, the SWNT/Si solar cells are drawing emerging attentions owing to their low cost and high efficiency [4-9]. The power conversion efficiencies (PCEs) of SWNT/Si solar cells have been improved an order of magnitude during last six years. However, the so-far-reported peak PCEs of the SWNT/Si solar cells were all suffered from

degradation, which is hindering their further applications. The SWNT/Si solar cells could lose almost 50% PCE after hours in air, and even with protection, the PCE still degraded by 20%. This could be attributed to that the peak PCEs were boosted by nitric acid or gold salt doping method which were unstable. Another issue remained controversial is the working mechanism of the SWNT/Si solar cells. Initially, the SWNT/Si solar cell was proposed as a *p*-*n* heterojunction [10]. However, the incident photon conversion efficiency (IPCE) spectrum of the SWNT/Si solar cells showed no obvious relationship with the SWNT absorption spectrum [5]. In addition, the efficiency of the graphene/Si solar cell became comparable with that of the SWNT/Si solar cells [11-13]. Thus, the SWNT/Si and graphene/Si solar cells were considered as a Schottky-barrier junction [13]. One characteristic that could distinguish the *p*-*n* junction and the Schottky-barrier junction is the effect of the interfacial oxide layer. For a conventional Schottky-barrier junction, inserting an interfacial oxide layer between the metal electrode and semiconductor would eliminate the pinning of Fermi level and thus improve the PCE, while the opposite case applies for a *p*-*n* junction. Until now, both significant improvement [6] and degradation [10] of the PCEs were observed after the removal of the interfacial oxide layer. These contradictory results call for more solid experimental proof for the further understanding of the SWNT/Si solar cells.

This article aims at improving the inherent performance of nanocarbon/Si solar cell through structural design to achieve air-stable high-efficiency solar cells. We focus on the development of SWNT microstructures which is suitable for the charge collection and transfer in solar cells and large-domain single-crystalline graphene which has superior electrical conductivity at high transparency. A novel water vapor treatment process is proposed to build up the as-synthesized vertically aligned SWNTs (VA-SWNTs) into a self-assembled hierarchical micro-honeycomb network (μ-HN). The condensation and evaporation of the water vapor on the VA-SWNTs resulted in the self-assembly process of μ-HN. The μ-HN SWNT film and the state-of-the-art

randomly oriented SWNT film were used for the SWNT/Si solar cells. The record-high fill factor (FF) of 72% was obtained for the pristine SWNT/Si solar cell using the μ-HN SWNT film. Moreover, the average size of the honeycomb cell in μ-HN decreases when the SWNT film becomes thinner. Such mechanism of μ-HN structure could avoid the tradeoff between the electrical conductivity and transparency and maintain the record high FF for thinner SWNT films. The performances of all the fabricated solar cells in this study were stable in the ambient environment for a year. The graphene/Si solar cells using milimeter-scale single-crystalline graphene have very similar performance as SWNT/Si solar cells. The high efficiency and stability demonstrated in this article make SWNT/Si and graphene/Si solar cells practical choices for next generation energy system.

Transparent Conductive Film with Dry-Deposited SWNTs

The randomly oriented SWNT films with high purity and long nanotube bundle length were synthesized by the aerosol CVD method [14]. The floating catalyst aerosol CVD was carried out in a scaled-up reaction tube with the diameter of 150 mm. Ferrocene vapor was thermally decomposed in the gas phase in the aerosol CVD reactor at the temperature of 880 ˚C. The CO gas was supplied at 4 L/min and decomposed on the iron nanoparticles, which resulted in the growth of SWNTs. As-synthesized SWNTs were collected by passing the flow through microporous filters at the downstream of the reactor. The transparency of the SWNT films was controlled by changing the collection time. The collected SWNT films can be transferred to arbitrary substrates through the dry transfer method, a sonication-free and surfactant-free process that could retain the excellent properties of SWNTs. The representative transferred SWNT film is shown in Figure 1(a) [8]. The SEM images (Figure 1(b)) demonstrates that the SWNT bundles

are well percolated in the film. Moreover, because of the surfactant-free transfer process, the high crystallinity of the SWNT was kept with over 40 G/D ratio. SWNT films with transparencies of 70%, 80% and 90% were used, which were named as TCF70, TCF80 and TCF90, respectively. The optical transmission spectra of the SWNT films are shown in Figure 1(d).

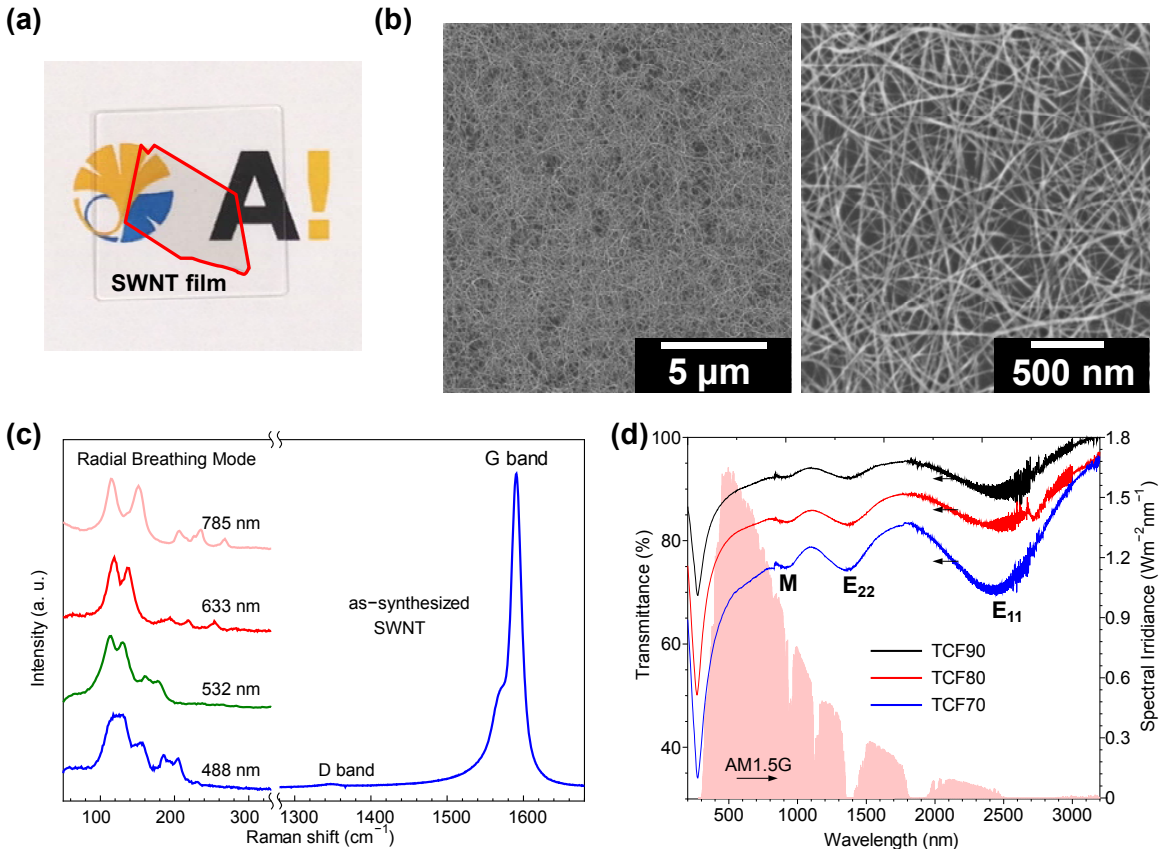

Figure 1 (a) An SWNT film on the fused quartz substrate after the dry-transfer process. (b) The SEM images at the low and high magnifications of the SWNT film from (a). (c) Raman spectra of the SWNT film under the laser excitation with the wavelength of 488 nm, 532 nm, 633 nm and 785 nm. (d) Transmission spectra of the TCF70, TCF80 and TCF90 SWNT films over the wavelength range of 200 nm to 3200 nm, with AM1.5G irradiance spectrum. Reproduced from Cui et al. (2014) [8].

Synthesis and Self-Assembly of Micro-Honeycomb SWNTs

VA-SWNTs were synthesized by the standard alcohol-catalytic CVD (ACCVD) method with Co/Mo dip-coated on quartz or Si/SiO_2 substrate [15]. The substrate loaded with Co/Mo bimetallic nanoparticle catalyst was placed in a quartz tube heated by an electric furnace after the dip-coating process and heated in a reduction environment gradually to 800 ˚C in 30 min. Then, the substrate was kept at 800 ˚C for 10 min before ethanol feedstock was introduced with the flow rate of 450 sccm at 1.3 kPa. The growth process of VA-SWNTs can be monitored by in-situ laser absorption technique for quartz substrate. The thickness of the VA-SWNT obtained from the in-situ laser absorption technique is consistent to that from the SEM cross-section measurement. With the controlled growth technique, we grew SWNTs on Si/SiO_2 substrate with the length of 5 μm. Moreover, the VA-SWNT films could be easily transferred onto any substrate by the hot-water method [16].

Self-assembly is a high-yield and low-cost method that builds low-dimensional materials into three-dimensional micro/macro-architectures with various morphologies. Capillary forces have been used to direct the self-assembling of patterned arrays of nanowires, nanopillars and multi-walled carbon nanotubes (MWNTs) into hierarchical networks [17]. However, due to the hydrophobicity and significantly smaller diameter of SWNTs, wetting vertically aligned SWNTs (VA-SWNTs) results in a high-density bulk with millimeter-scale cracks rather than the hierarchical honeycomb-like network formed by MWNT arrays [18]. So far, such a honeycomb structure of SWNTs has been achieved only by film-casting anionic shortened SWNTs–cationic ammonium lipid conjugates in organic solution [19], of which the complicated solution preparation induced defects and degradation of SWNTs.

After the synthesis of the high-quality VA-SWNTs, the water vapor treatment includes two steps: (1) expose the VA-SWNT array to vapor from a hot water reservoir, and (2) turn the

substrate over and dry the array in the ambient environment, as shown in Figure 2(a) [7]. The uniform VA-SWNT array (Figure 2(b)) was aggregated into hexagonal frames (Figure 2(c)) after the first water vapor treatment. By repeating this treatment, the VA-SWNT array evolved into a micro-honeycomb network (μ-HN) after 20 iterations, as shown in Figure 2(d). The liquid-solid interaction induced by the condensation and subsequent evaporation of water is the building tool used to engineer the morphology of VA-SWNTs into a self-assembled μ-HN. The μ-HN is a hierarchical hexagonal-shaped three-dimensional network (Figure 3(a)) that consists of vertical SWNT walls and a randomly networked SWNT bottom. Each wall is a cross-linked high-density SWNT agglomeration (Figure 3(b)), and the bottom of each honeycomb cell is a randomly oriented buckypaper, which results from the collapse of SWNT alignment. The most energetically favorable outcome is a honeycomb network because it uniformly divides the region into cells having minimal perimeter, *i.e.*, allows the largest number of SWNTs to collapse.

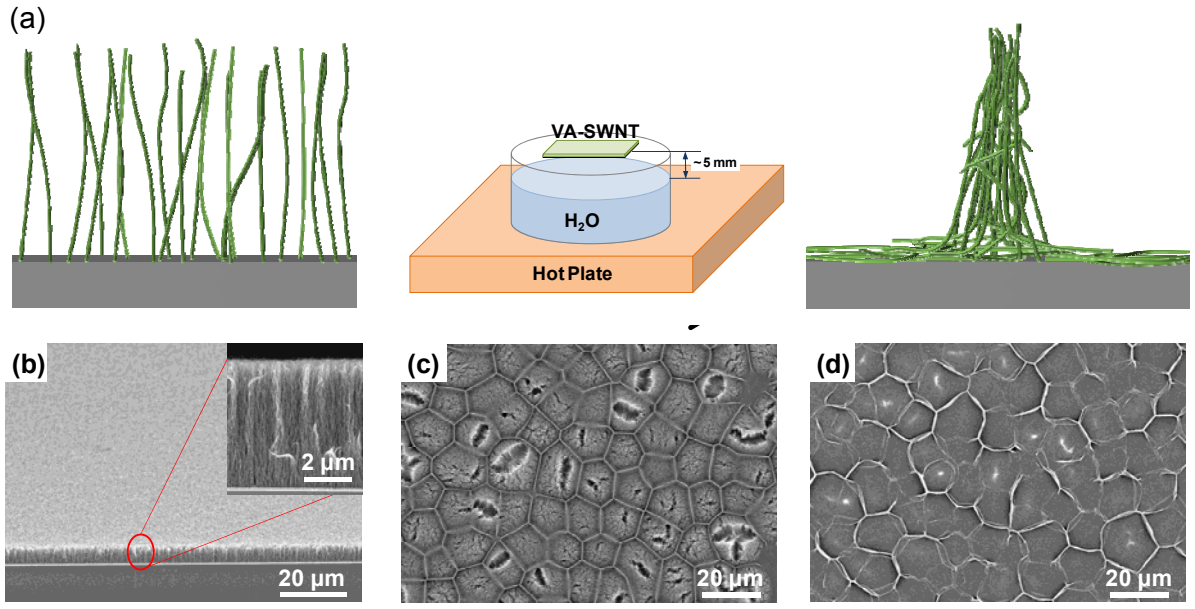

Figure 2 Water vapor treatment of the VA-SWNT array into a μ-HN. (a) Schematic of the water vapor treatment process. (b) As-synthesized high-quality VA-SWNT with a uniform top surface. (c) Intermediate

stage of the μ-HN formation after the first vapor exposure. (d) Stable μ-HN formed after 20 times iteration of the water vapor treatment**.** Reproduced from Cui et al. (2013) [7]**.**

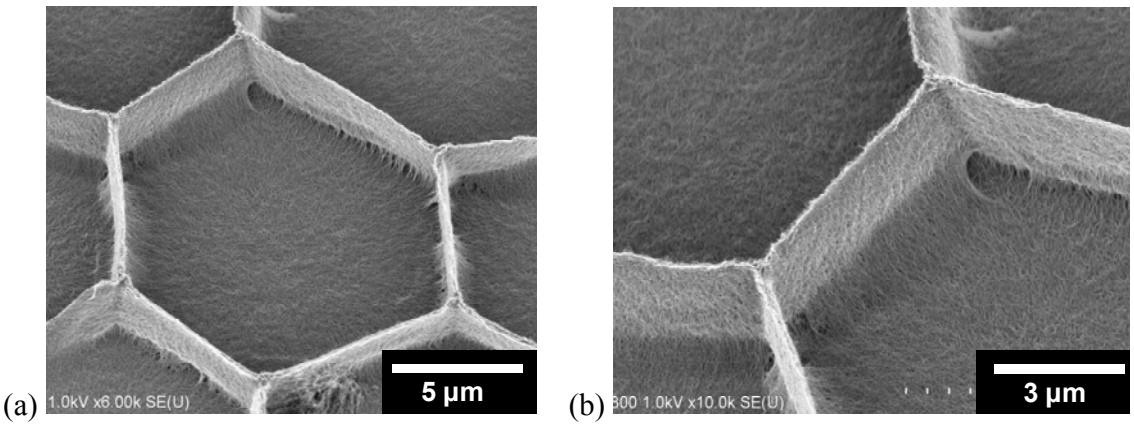

Figure 3 (a) An individual honeycomb cell. (b) Magnified image of the hierarchical structure of μ-HN. The walls are a cross-linked highly-condensed SWNT agglomeration. The bottom of each honeycomb cell is a randomly oriented buckypaper.

Fabrication of SWNT/Si Solar Cells

Each SWNT/Si solar cell was fabricated by transferring the SWNT film onto a designed substrate, which was composed of a 3 mm × 3 mm *n*-type Si contact window and surrounding electrodes. The *n*-type Si (SUMCO Inc.) has the series resistance of 10 ± 2.5 Ω/cm with the dopants concentration of ~10^{15} m^{-3}. The fabrication process of the Si substrate for the SWNT/Si solar cell is given in Figure 4(a). Before the metal deposition, the *n*-type Si substrate was consequentially treated with RCA1, 5 M NaOH and RCA2 solution for the removal of organics, oxide layer and impurity metals. After the cleaning treatment, a very thin oxide layer was formed with the thickness of 6 Å ~ 7 Å, according to the measurement of X-ray photoelectron spectroscopy (XPS, PHI 5000 VersaProbe) [8]. The 3 mm × 3 mm physical masks were patterned on the top surface of the Si substrate before the metal deposition. A 200-nm-thick SiO_2 insulator layer and a 50-nm-thick Pt electrode were subsequently RF-sputtered (ULVAC-RIKO,

Inc.) on the top surface of the Si substrate. The Ti film with the thickness of 10 nm was selected as the back electrode for the lineup of the band structure. The SWNT films were transferred onto the top surface of Si substrate after the removal of the physical masks. The schematic of the fabricated SWNT/Si solar cell is shown in Figure 4(b). The photograph of the SWNT/Si solar cells with micro-honeycomb structure and random-oriented network is shown in Figure 4(c).

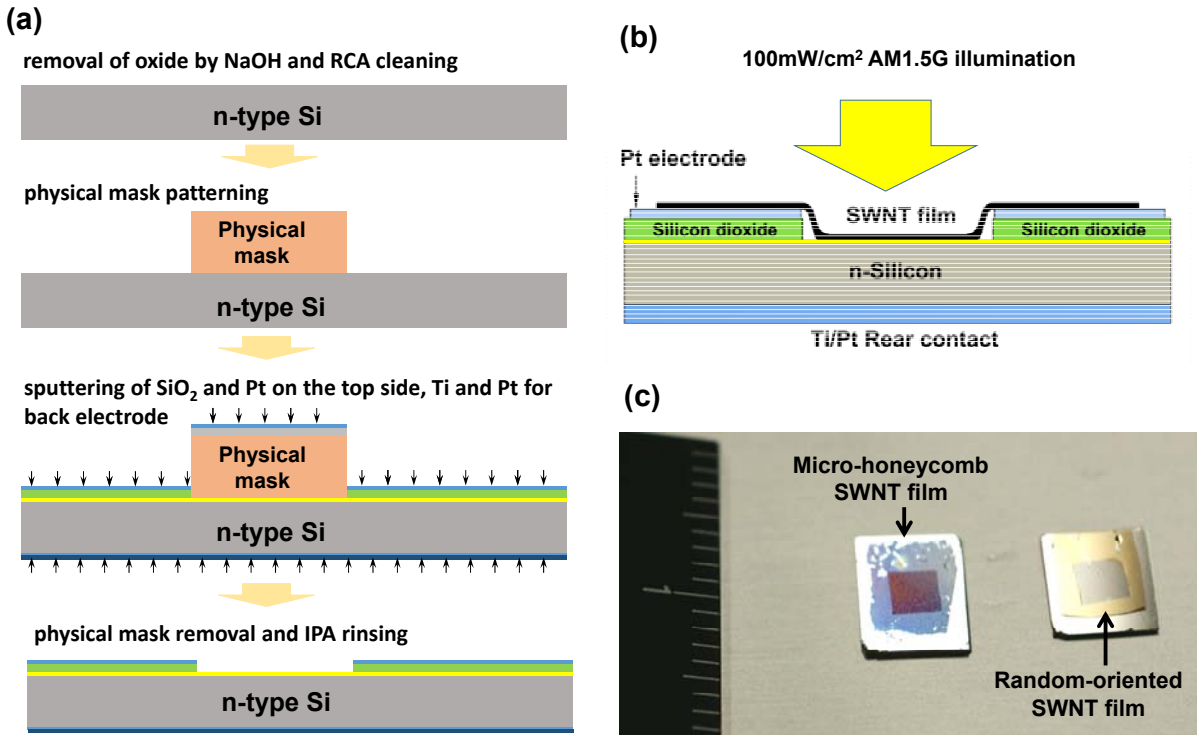

Figure 4 (a) Fabrication process of the *n*-type Si substrate for the SWNT/Si solar cell. (b) Schematic of the SWNT/Si solar cell. (c) Photograph of the SWNT/Si solar cells with micro-honeycomb structure and random-oriented network.

Experimental Performance and Modeling of SWNT/Si Solar Cells

The *J-V* characteristics of the SWNT/Si solar cells using random-oriented SWNT films was examined under AM1.5G 100 mW/cm^2 illumination (PEC-L01, Peccell Technologies, Inc.), as shown in Figure 5(a). The obtained peak PCE value was 10.1% for the SWNT films with

transparency of 90% [8]. The PCE value is comparable to the SWNT/Si solar cells doped with nitric acid and/or gold salt in the previous literatures [4-6, 9]. The superiority of the PCE over the previous reports is attributed to the well-retained high crystallinity, long tube length of the SWNTs as well as the sound inter-SWNT and SWNT-Si contact. More importantly, the *J-V* characteristics underwent almost no change in the ten-month duration in the ambient. The open-circuit photovoltage (V_{oc}) values increased by 13 mV to 550 mV. This can be attributed to the oxygen modification to the SWNT films, which would *p*-dope SWNTs [20] and shift the Fermi level downwards. This would further enlarge the built-in voltage, leading to the increase of V_{oc}. We also spin-coated PMMA layer on top of the SWNT film as antireflection layer and dopant of SWNTs. As shown in Figure 5(b), both the short-circuit photocurrent (J_{sc}) and V_{oc} were increased, resulting in a significant improvement of PCE from 8.93% to 11.15%. The PCE was slightly decreased after the solar cell was exposed in the ambient condition for one week. The quantitative values of the PMMA-coated SWNT/Si solar cells are given in Table 1.

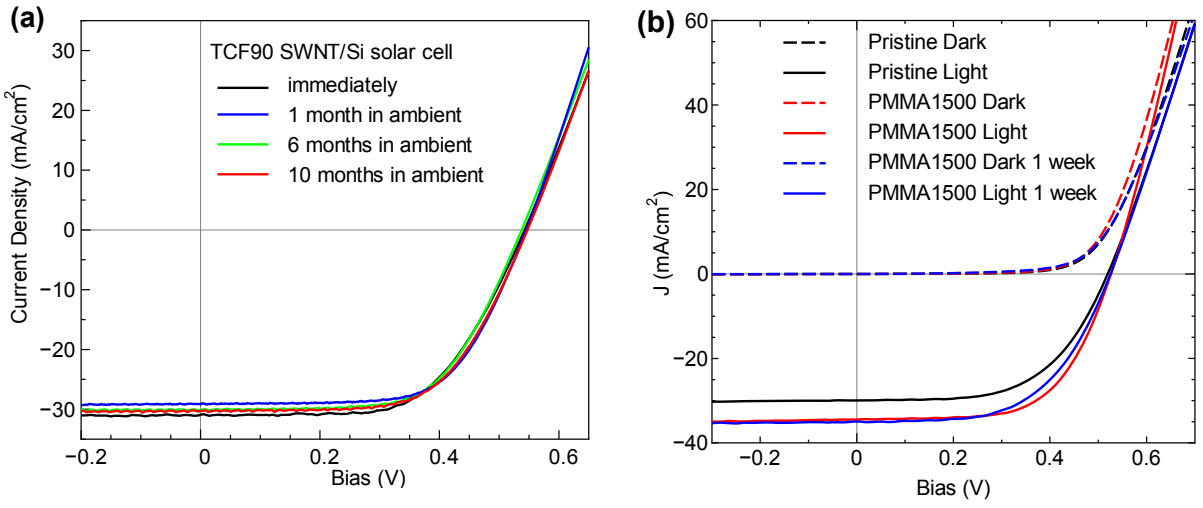

Figure 5 (a) *J-V* characteristics of the SWNT/Si solar cell using TCF90 film measured immediately as well as after 1, 6 and 10 months exposed in the ambient condition. (b) *J-V* characteristics of the SWNT/Si solar cell

using TCF90 film with PMMA coating measured immediately as well as after one week exposed in the ambient condition

Table 1 Solar cell characteristics (PCE, FF, J_{sc}, V_{oc}) of pristine SWNT/Si solar cell and PMMA/SWNT/Si solar cells.

	PCE (%)	FF (%)	J_{sc} (mA/cm^2)	V_{oc} (mV)
Pristine SWNT/Si	8.93	57.3	29.97	520
PMMA/SWNT/Si	11.15	61.7	34.44	527
PMMA/SWNT/Si after 1 week	10.40	56.5	34.94	525

SWNT/Si Solar Cells with Micro-Honeycomb SWNTs

The pristine μ-HN SWNT/Si solar cell exhibited the highest and stable FF of 72%, with an ideality factor of 1.71 over the 300 to 500 mV range, as shown in Figure 6(a) [7]. This ideality factor is the lowest reported so far (*i.e.*, closest to an ideal device). The PCE of 5.91% was obtained immediately after the fabrication, and it gradually increased to 6.04% after three weeks in ambient condition. The FF represents the quality of a solar cell, which is independent of V_{oc} and J_{sc}. The significant improvement in FF and ideality factor over previously reported values is attributed to the hierarchical μ-HN, which simultaneously enhances carrier generation, separation, collection and transport. A doping process was then carried out by dropping 120 μL of 2.4 M nitric acid onto the device which was heated to 50 ˚C using a hot plate. The μ-HN structure remains almost unchanged after the acid doping process. After drying, the PCE reached 10.02%, with an even higher FF of 73%. The *J-V* characteristics of the SWNT/Si solar cells after

doping are also shown in Figure 6(a). The open-circuit voltage and short-circuit current after doping increased to 0.55V and 25.01 mA/cm^2, respectively. The PCE value of the μ-HN SWNT/Si solar cell decreased to 9.29% after 12 hours, which may be attributed to accelerated oxidation at the Si surface. A substantial increase in the transmittance spectrum from 600 nm to 1200 nm (Figure 6(b)) and a five-fold decrease in the sheet resistance (from 614 Ω/sq. to 105 Ω/sq., as shown in Figure 6(c) contribute to the increase of the PCE. The dramatic changes in the electrical and the optical properties result from charge transfer from the SWNTs induced by the nitric acid. Depletion of electrons from the valence band results in a shift in the Fermi level and the attenuation of absorption peaks. The decrease of sheet resistance may be also attributed to further bundling of SWNTs. The heavy doping and increased bundling may make some semiconducting SWNTs exhibit metallic behavior.

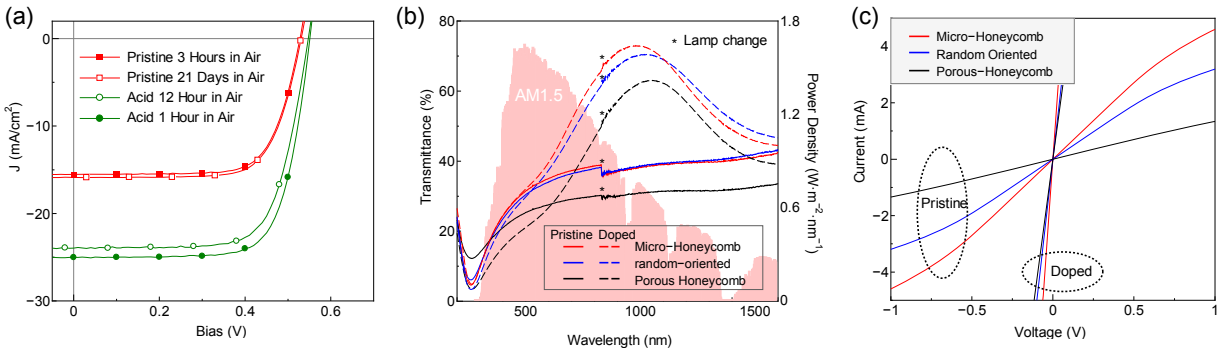

Figure 6 (a) *J-V* characteristics of a micro-honeycomb structured SWNT/Si solar cell measured three hours and 21 days after device fabrication (shown in red), as well as 1 h and 12 h after dilute nitric acid doping (shown in green). (b) UV-vis-NIR transmittance spectra of μ-HN, collapsed HN and porous HN for pristine (solid) and doped (dashed) conditions. (c) Sheet resistance of μ-HN, collapsed HN and porous HN structures before and after acid doping. Reproduced from Cui et al. (2013) [8]**.**

Through varying the thickness of the VA-SWNT film, the average size of the honeycomb cell can be changed accordingly. We compared the honeycomb structure of a 5 μm-thick and a 2.5

μm-thick VA-SWNT film. As shown in the inset of Figure 7(a), after the water vapor treatment, the honeycomb cells are much smaller for the 2.5 μm-thick VA-SWNT film compared with the 5 μm-thick one. The two honeycomb structured films were then transferred onto *n*-type Si substrate to form heterojunction solar cell. As shown in Figure 7(a), the thinner honeycomb film with finer honeycomb cell size could significantly improve the performance of solar cells, with the PCE value increased from 6.01% to 8.05%. More importantly, degradation of FF value which has been widely observed for the random-oriented SWNTs/Si solar cells does not exist for honeycomb structured SWNT/Si solar cells. This suggests that compared with random-networked SWNT film, the honeycomb structured SWNT film could overcome the tradeoff of transparency and conductivity of transparent conductive films to a certain extent. We expect further decrease in the thickness of the VA-SWNT film could improve the performance of SWNT/Si solar cell.

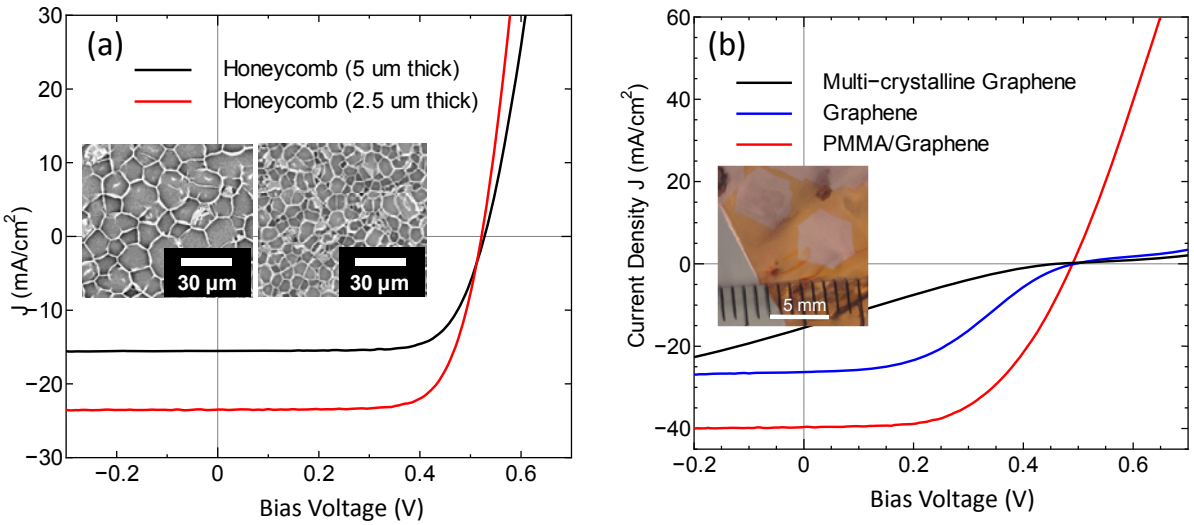

Figure 7 (a) *J-V* characteristics of a micro-honeycomb structured SWNT/Si solar cell with different thickness and honeycomb cell size. (b) *J-V* characteristics of graphene/Si solar cell with different single-crystalline domain size.

Graphene/Si Solar Cells with Large-Scale Single Crystal Graphene

We synthesized large-domain graphene using alcohol catalytic CVD method discussed in detail elsewhere [21]. The graphene was then transferred onto Si substrate with spin-coated PMMA layer. The PMMA layer was kept intentionally after the transfer process, which could protect the graphene from tearing apart. As shown in Figure 7(b), the 5 mm-scale single-crystalline graphene demonstrated a substantial improvement in solar cell performance compared with multicrystalline graphene, with the PCE increased from 1.50% to 5.14%. With the coating of PMMA, the PCE of the graphene/Si solar cell further increased to 11.37%. The increase of in all the three parameters, *i.e.* J_{sc}, V_{oc} and FF could be observed. We expect that large-domain single-crystalline graphene is very promising in the application of Si heterojunction solar cells.

Films of SWNTs for Organic Solar Cells and Perovskite Solar Cells

Films of SWNTs network are promising flexible transparent-conductive layer for other kind of solar cells. In addition, we found that SWNT film or doped graphene can behave as a stable conductive electron blocking layer (EBL). We have demonstrated these characteristics in honeycomb-structured SWNTs-Si solar cells [7], dry-deposited SWNTs-Si solar cells [8], graphene-Si solar cells, organic solar cell (OSC) [22, 23], and perovskite-type solar cells [24]. For organic solar cells, the SWNT/MoOx/PEDOT:PSS nanocomposite was proposed and developed as electron blocking layer and electrode replacing ITO. Using PTB7/PC71BM mixture as active materials, the PCE of 6% was obtained for on glass substrate and 3.9% on flexible PET substrate [22]. By using SWNT film as the top electrode of inverted type OSC, window-like OSC can be fabricated with reasonable PCE [23]. The electron blocking and

electrode function of SWNTs was also demonstrated in normal and inverted type [24] perovskite solar cells with over 9% PCE.

Summary

In this study, both SWNTs and graphene have been utilized to form heterojunctions with Si for solar energy conversion. Air-stable beyond-10%-efficiency nanocarbon/Si solar cells have been achieved. We also proposed future direction to further optimize the performance of SWNT/Si and graphene/Si solar cells, including refining the honeycomb structure of SWNTs and increasing domain size of single-crystalline graphene. Multi-functionalizing polymer layer, PMMA is found to effectively increase the FF, J_{sc} and V_{oc} at the same time, resulting in the significantly improvement of the solar cell performance.

Acknowledgements

This work was financially supported by JSPS KAKENHI Grant-in-Aid for Scientific Research (25107002, 15H05760), Grant-in-Aid for Young Scientists (15K17983) and JST-EC DG RTD Coordinated Research Project 'IRENA' under the Strategic International Collaborative Research Program (JST-SICORP).

References

[1] Ph. Avouris and M. Freitag, “Carbon-nanotube photonics and optoelectronics,” *Nat. Photonics*, vol. 2, pp. 341–350, 2008.

[2] J. Zhao, A. Wang, M. A. Green and F. Ferreazza, “19.8% efficient “honeycomb” textured multicrystalline and 24.4% monocrystalline silicon solar cells,” *Appl. Phys. Lett.*, vol. 73, pp.1991–1993, 1998

[3] M. A. Green, K. Emery, Y. Hishikawa, W. Warta, E. D. Dunlop, “Solar cell efficiency tables (version 46)”, *Prog. Photovoltaics: Res. Appl.*, vol. 23, pp. 805-812, 2015

[4] J. Wei, Y. Jia, Q. Shu, Z. Gu, K. Wang, D. Zhuang, G. Zhang, Z. Wang, J. Luo, A. Cao and D. Wu, “Double-walled carbon nanotube solar cells,” *Nano Lett.*, vol. 7, pp. 2317–2321, 2007.

[5] Y. Jia, A. Cao, X. Bai, Z. Li, L. Zhang, N. Guo, J. Wei, K. Wang, H. Zhu, D. Wu, P. M. Ajayan, “Achieving high efficiency silicon-carbon nanotube heterojunction solar cells by acid doping,” *Nano Lett.*, vol. 11, pp. 1901–1905, 2011.

[6] Y. Jung, X. Li, N. K. Rajan, A. D. Taylor, M. A. Reed, “Record High Efficiency Single-Walled Carbon Nanotube/Silicon p–n Junction Solar Cells,” *Nano Lett.*, vol. 12, pp. 95–99, 2012.

[7] K. Cui, T. Chiba, S. Omiya, T. Thurakitseree, P. Zhao, S. Fujii, H. Kataura, E. Einarsson, S. Chiashi, S. Maruyama, “Self-assembled microhoneycomb network of single-walled carbon nanotubes for solar cells,” *J. Phys. Chem. Lett.*, vol. 4, pp. 2571-2576, 2013

[8] K. Cui, A. S. Anisimov, T. Chiba, S. Fujii, H. Kataura, A. G. Nasibulin, S. Chiashi, E. I. Kauppinen, S. Maruyama, “Air-stable high-efficiency solar cells with dry-transferred single-walled carbon nanotube films,” *J. Mater. Chem. A*, vol. 2, pp. 11311-11318, 2014.

[9] F. Wang, D. Kozawa, Y. Miyauchi, K. Hiraoka, S. Mouri, Y. Ohno and K. Matsuda, “Considerably improved photovoltaic performance of carbon nanotube-based solar cells using metal oxide layers,” *Nat. Comm.*, vol. 6, pp. 6305, 2015.

[10] Y. Jia, J Wei, K. Wang, A. Cao, Q. Shu, X. Gui, Y. Zhu, D. Zhuang, G. Zhang, B. Ma, L. Wang, W. Liu, Z. Wang, J. Luo, D. Wu, “Nanotube–silicon heterojunction solar cells,” *Adv. Mater.*, vol. 20, pp. 4594–4598, 2008.

[11] X. Miao, S. Tongay, M. K. Petterson, K. Berke, A. G. Rinzler, B. R. Appleton, and A. F. Hebard, “High efficiency graphene solar cells by chemical doping,” *Nano Lett.*, vol. 12, pp. 2745–2750, 2012.

[12] E. Shi, H. Li, L. Yang, L. Zhang, Z. Li, P. Li, Y. Shang, S. Wu, X. Li, J. Wei, K. Wang, H. Zhu, D. Wu, Y. Fang, A. Cao, “Colloidal antireflection coating improves graphene-silicon solar cells.” *Nano Lett.*, vol. 13, pp. 1776–1781, 2013.

[13] Y. Song, X. Li, C. Mackin, X. Zhang, W. Fang, T. Palacios, H. Zhu, J. Kong, “Role of Interfacial Oxide in High-Efficiency Graphene-Silicon Schottky Barrier Solar Cells,” *Nano Lett.*, vol. 15, pp. 2104-2110, 2015.

[14] A. G. Nasibulin, A. Kaskela, K. Mustonen, A. S. Anisimov, V. Ruiz, S. Kivistö, S. Rackauskas, M. Y. Timmermans, M. Pudas, B. Aitchison, M. Kauppinen, D. P. Brown, O. G. Okhotnikov, E. I. Kauppinen, “Multifunctional freestanding single-walled carbon nanotube films,” *ACS Nano*, vol. 5, pp. 3214–3221, 2011.

[15] Y. Murakami, S. Chiashi, Y. Miyauchi, M. Hu, M. Ogura, T. Okubo, S. Maruyama, “Growth of vertically aligned single-walled carbon nanotube films on quartz substrates and their optical anisotropy,” *Chem. Phys. Lett.*, vol. 385, pp. 298–303, 2004.

[16] Y. Murakami, S. Maruyama, “Detachment of vertically aligned single-walled carbon nanotube films from substrates and their re-attachment to arbitrary surfaces,” *Chem. Phys. Lett.*, vol. 422, pp. 575–580, 2006.

[17] M. De Volder, A. J. Hart, “Engineering hierarchical nanostructures by elastocapillary self-assembly,” *Angew. Chem., Int. Ed.*, vol. 52, pp. 2412–2425, 2013.

[18] D. N. Futaba, K. Hata, T. Yamada, T. Hiraoka, Y. Hayamizu, Y. Kakudate, O. Tanaike, H. Hatori, M. Yumura, S. Iijima, “Shape-engineerable and highly densely packed single-walled carbon nanotubes and their application as super-capacitor electrodes,” *Nature Mater.*, vol. 5, pp. 987–994, 2006.

[19] H. Takamori, T. Fujigaya, Y. Yamaguchi, N. Nakashima, “Simple preparation of self-organized single-walled carbon nanotubes with honeycomb structures,” *Adv. Mater.*, vol. 19, pp. 2535–2539, 2007.

[20] W. Zhou, J. Vavro, N. M. Nemes, J. E. Fischer, F. Borondics, K. Kamarás and D. B. Tanner, “Charge transfer and Fermi level shift in p-doped single-walled carbon nanotubes,” *Phys. Rev. B*, vol. 71, pp. 205423, 2005.

[21] X. Chen, P. Zhao, R. Xiang, S. Kim, J. Cha, S. Chiashi, S. Maruyama, “Chemical vapor deposition growth of 5 mm hexagonal single-crystal graphene from ethanol”, *Carbon*, vol. 94, pp. 810-815, 2015.

[22] I. Jeon, K. Cui, T. Chiba, A. S. Anisimov, A. G. Nasibulin, E. I. Kauppinen, S. Maruyama, Y. Matsuo, “Direct and Dry Deposited Single-Walled Carbon Nanotube Films Doped with MoOx as Electron-Blocking Transparent Electrodes for Flexible Organic Solar Cells,” *J. Am. Chem. Soc.*, vol. 137, pp. 7982-, 2015.

[23] I. Jeon, C. Delacou, A. Kaskela, E. I. Kauppinen, S. Maruyama, Y. Matsuo, “Metal-electrode-free Window-like Transparent Organic Solar Cells with P-dopant Enhanced Carbon Nanotube Thin-film Electrodes,” submitted, 2015.

[24] I. Jeon, T. Chiba, C. Delacou, Y. Guo, A. Kaskela, O. Reynaud, E. I. Kauppinen, S. Maruyama, Y. Matsuo, “Single-Walled Carbon Nanotube Film as Electrode in Indium-Free Planar Heterojunction Perovskite Solar Cells: Investigation of Electron-Blocking Layers and Dopants,” *Nano Lett.*, vol. 15, pp. 6665-6671, 2015.